2022

Quantifying Seasonal Particulate Organic Carbon Concentrations and Export Potential in the Southwestern Ross Sea Using Autonomous Gliders

Meredith G. Meyer
Virginia Institute of Marine Science

Randolph G. Jones

Walker O. Smith Jr.
Virginia Institute of Marine Science

Recommended Citation

Meyer, Meredith G.; Jones, Randolph G.; and Smith, Walker O. Jr., Quantifying Seasonal Particulate Organic Carbon Concentrations and Export Potential in the Southwestern Ross Sea Using Autonomous Gliders (2022). *JCR Oceans*, 12710(e2022JC018798).
doi: 10.1029/2022JC018798

JGR Oceans

RESEARCH ARTICLE
10.1029/2022JC018798

Quantifying Seasonal Particulate Organic Carbon Concentrations and Export Potential in the Southwestern Ross Sea Using Autonomous Gliders

Meredith G. Meyer[1], Randolph M. Jones[2], and Walker O. Smith Jr.[1,3]

[1]Virginia Institute of Marine Science, College of William & Mary, Williamsburg, VA, USA, [2]United States Antarctic Program, Antarctic Support Contract, Centennial, CO, USA, [3]School of Oceanography, Shanghai Jiao Tong University, Shanghai, China

Abstract To assess the temporal biological and hydrographic features of the southwestern Ross Sea, we deployed a glider in a spatially restricted, ice-free area during the austral summer (1 December–6 February), and quantified from sensor measurements the particulate organic carbon (POC; via particulate backscatter) concentrations, their changes through time, and net community production (NCP; via dissolved O_2 concentrations). The POC levels could be divided into three distinct phases (I, II, and III, respectively) characterized by changes in NCP, surface-layer POC concentrations, remineralization, and export. Surface POC concentrations increased from 215 mg C m^{-3} in early December to a peak of >400 mg C m^{-3} by mid-December, before decreasing to 227 mg C m^{-3} in late January–early February. NCP was highly variable throughout the summer, becoming maximal in mid-December. By constructing a carbon budget, we estimated rates of change of POC and export potential to the mesopelagic in each phase. Changes in euphotic zone POC concentrations and NCP suggested that the system is slightly net autotrophic during the observational period (average NCP is 0.05 g C m^{-2} d^{-1}), and POC removal from the top 240 m of the water column averaged 0.22 g C m^{-2} d^{-1}. Our data confirm that the southern Ross Sea during the ice-free season is a high productivity, low export system while providing high-resolution POC dynamics that had not been previously observed. Although the Ross Sea is a site of substantial carbon fixation, there remains an incomplete understanding both of the processes involved in export and the rates and controls of remineralization.

Plain Language Summary The Ross Sea, Antarctica is a remote region of the Southern Ocean that has been shown to support a predictable, large growth, and accumulation of photosynthetic microorganisms (phytoplankton). This bloom is an ecologically important feature for understanding the global climate cycle, as it is believed to account for 28% of the carbon fixation in the Southern Ocean. The annual bloom is composed of two types of phytoplankton: the gelatinous *Phaeocystis antarctica* and siliceous diatoms. Understanding the characteristics of the bloom is important to understand how much carbon is removed (i.e., sequestered) from the upper ocean and to quantify the role of this region in the global carbon cycle. An autonomous vehicle was deployed in 2012–2013 to measure changes in concentrations of particulate organic carbon (POC) and dissolved oxygen over the course of the bloom. Results suggest high yet variable rates of net community production and fine-scale changes both in time and space in POC in the upper 240 m of the ocean, suggestive of substantial microbial degradation of POC. This high-resolution analysis indicates this region is highly productive but does not export substantial quantities of organic carbon during the ice-free season.

Key Points:

- Glider surveys provide high resolution data to enhance patterns in carbon cycle processes during the southwestern Ross Sea productive period
- Substantial remineralization occurs and drives carbon removal processes in the austral spring and summer
- Net community production and particulate organic carbon changes characterize the region as a high productivity, high export potential system

Supporting Information:

Supporting Information may be found in the online version of this article.

Correspondence to:

M. G. Meyer,
mgmeyer9@email.unc.edu

Citation:

Meyer, M. G., Jones, R. M., & Smith, W. O. Jr. (2022). Quantifying seasonal particulate organic carbon concentrations and export potential in the southwestern Ross Sea using autonomous gliders. *Journal of Geophysical Research: Oceans*, *127*, e2022JC018798. https://doi.org/10.1029/2022JC018798

Received 4 MAY 2022
Accepted 20 SEP 2022

Author Contributions:

Conceptualization: Meredith G. Meyer, Walker O. Smith
Data curation: Meredith G. Meyer, Randolph M. Jones
Formal analysis: Meredith G. Meyer, Randolph M. Jones, Walker O. Smith
Funding acquisition: Walker O. Smith
Investigation: Meredith G. Meyer, Randolph M. Jones, Walker O. Smith
Methodology: Meredith G. Meyer, Walker O. Smith
Resources: Walker O. Smith

1. Introduction

Having an accurate measure of how much organic carbon is exported from the surface layer to depth is crucial in developing an accurate global carbon budget for today and the future. The Southern Ocean is a critical region for both inorganic and organic carbon fluxes (Le Quére et al., 2007), and as such, its particulate organic carbon (POC) export is essential to quantify. It is markedly different from temperate and tropical oceans, given its low temperatures and pulsed, seasonally variable phytoplankton stocks and production. Productivity in the Southern Ocean is greatest on the continental shelves (Arrigo & van Dijken, 2004), and among all continental shelves, the Ross Sea is the most productive (Smith, Ainley, et al., 2014). It is estimated to be responsible for 28% of Southern Ocean carbon fixation (Arrigo et al., 2008) and supports substantial abundances of higher trophic levels (Smith, Ainley, et al., 2014). It is also the site of a large amount of organic matter export to depth (e.g., Collier et al., 2000;

Supervision: Walker O. Smith
Validation: Meredith G. Meyer, Walker O. Smith
Visualization: Meredith G. Meyer, Walker O. Smith
Writing – original draft: Meredith G. Meyer
Writing – review & editing: Meredith G. Meyer, Walker O. Smith

Nelson et al., 1996). While the importance of the Ross Sea to the Antarctic carbon cycle has been established, the mechanisms, rates and processes involved in carbon export and remineralization remain poorly constrained (Gruber et al., 2019).

The seasonal features of the Ross Sea's biogeochemistry and oceanography are relatively well known. Phytoplankton begin to grow in early spring (late October) as solar radiation increases in the water column as a result of the lengthening photoperiod, the reduction in ice cover, and the shoaling of stratification within the water column (Arrigo & van Dijken, 2003; Smith & Gordon, 1997). The austral spring bloom is dominated by the haptophyte *Phaeocystis antarctica*, which reaches its maximum biomass in mid to late December (chlorophyll concentrations can exceed 15 μg L^{-1}; Smith et al., 2000; Smith, Asper, et al., 2011). *P. antarctica* exists largely as colonies (up to 2 mm in diameter; Mathot et al., 2000), and its biomass in the euphotic zone after the December maximum is rapidly reduced over a period of days to weeks (Jones & Smith, 2017; Smith et al., 2000). During summer, diatoms can reach a biomass similar to that of *P. antarctica* during spring, although substantial interannual variations in diatom abundance apparently occur (Smith, Asper, et al., 2011). The role of diatoms in annual productivity has recently been reassessed, and it was concluded that diatoms contribute a large majority (ca. 75%) of the annual production (Smith & Kaufman, 2018).

Previous studies have estimated Ross Sea organic carbon fluxes through the use of sediment traps and thorium-234 budgets (Cochran et al., 2000; Collier et al., 2000; Dunbar et al., 1998; Smith, Shields, et al., 2011), but the accuracy of these methods is uncertain (Buesseler & Boyd, 2009). These measurements of export also do not generally provide vertical resolution within the water column, as often only a single sediment trap is deployed at one location and depth, and use of thorium is constrained by the need to filter water samples at discrete depths. Furthermore, as bottom-moored sediment traps often sample to resolve annual patterns, the temporal resolution of such methods is limited. Increasing temporal resolution is of particular interest in regions with marked seasonal pulses, such as the Ross Sea. The increasingly common use of autonomous underwater vehicles, such as gliders, allows for data collection with increased spatial and temporal resolution (Alkire et al., 2014; Kaufman et al., 2014; B. Y. Queste et al., 2015; Smith, Goetz, et al., 2014). For example, Kaufman et al. (2018) assimilated glider data into a 3-D model to estimate vertical POC export in the Ross Sea, and also predicted the impacts of climate change on this export. Using glider data and its increased temporal and spatial resolution has provided improved understanding of the changes in surface level biomass, the influence of short-term events (perturbations) on POC concentrations, and the local hydrography (Kaufman et al., 2014; Smith, Goetz, et al., 2014).

To assess POC export and net community production (NCP), we used high-resolution autonomous glider data (oxygen, fluorescence, and optical backscatter data, with the latter two converted to chlorophyll and POC concentrations, respectively) collected during 2012–2013 in the southern Ross Sea, Antarctica. As summer progressed, there was a reduction in average productivity and a vertical deepening of the maximum POC concentration (Jones & Smith, 2017). We calculated vertical distributions of POC and rates of NCP to estimate continuous inputs of organic matter into the euphotic zone via photosynthesis, the potential export of organic matter to depth, and its remineralization within the water column. Given the increasingly common use of gliders in oceanographic studies, such an approach can provide export and remineralization estimates from a variety of oceanic systems and reduce the uncertainty of our present estimates of these critical variables. Quantifying these variables will allow development of more accurate productivity-export models and a better understanding of the role of the Ross Sea in Southern Ocean carbon cycling.

2. Methods

2.1. Glider Analyses

Data for this study were collected as part of the 2012–2013 Glider Observations of Variability in the Ross Sea project (Figure 1). We used an iRobot Seaglider™ (Model: 1KA; serial number SG503) equipped with a Seabird CT Sail, an Aanderaa 4330F oxygen Optode, a Wet Labs ECO Triplet Puck, and an Imagenex 853 Echo Sounder. Glider deployment was on 22 November 2012 at 09:25 UTC from the fast ice near Ross Island (77.438°S, 169.746°E), and recovery occurred on 8 February 2013 at 00:44 UTC at 76.77°S, 167.729°E from the *RVIB Nathaniel B. Palmer* (Jones & Smith, 2017). The optical puck was turned off below 250 m to conserve battery power. Euphotic zone depths were estimated via chlorophyll concentration using the relationships described by Morel (1974), as no PAR sensor was mounted on the glider. Mixed layer depths were estimated by a 0.02 kg

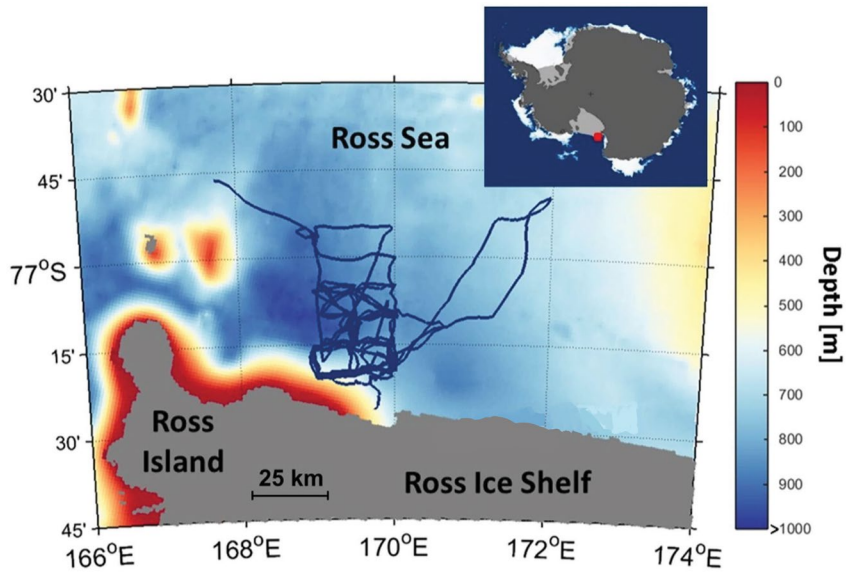

Figure 1. Map of the 2012–2013 glider track (blue line) in the southwestern Ross Sea. The glider was deployed for a total of 79 days in austral summer and completed 923 dives. The red mark in the inset shows the location within the Ross Sea. Modified from Jones (2015).

m^{-3} change in density relative to the average density for the top 10 m on each of the dives (Ryan-Keogh & Smith, 2021). All data are available at https://www.bco-dmo.org/project/566865.

Based on the surface characteristics of chlorophyll and POC, we divided the study period into three phases as has been previously done in other studies (Jones & Smith, 2017; Ryan-Keogh & Smith, 2021). Phase I (from 1 December to 15 December) was characterized by increasing phytoplankton biomass and variable NCP in the surface layer, whereas Phase II (from 16 December to 7 January) was delineated by relatively constant levels of POC and chlorophyll and high rates of NCP. Phase III (from 8 January to 6 February) was characterized by overall declining NCP and reduced surface layer biomass levels and substantial surface layer variability.

Dissolved oxygen concentrations were measured using an Optode, which was factory calibrated before deployment. Dissolved oxygen concentrations were further calibrated against CTD profiles collected on the *RVIB Palmer* ($n = 204$; $R^2 = 0.76$; $p < 0.01$), corrected for salinity and processed according to the "uea-seaglider-toolbox" (created by Dr. B. Queste, 2015), as well as corrected for error via manual inspection (Figure S1 in Supporting Information S1). The post-deployment oxygen residual on the Optode as calculated by Sea-Bird was 1.00 mL L^{-1} (Figure S2 in Supporting Information S1).

POC concentrations were estimated by conversion of glider optical backscattering counts ($b_{b_p}[\lambda]$) calibrated using discrete measurements of POC from casts taken upon deployment and recovery of the glider (Figure S3 in Supporting Information S1). Optical backscattering values were converted to total volume scattering (b_{b_p}) by multiplying by a factory-calibrated scale factor, subtracting the volume scattering of seawater (Morel, 1974) and multiplying by $2\pi\chi$, where χ is 1.1 (Boss & Pegau, 2001). The regression used was

$$\mathrm{POC} = \left(42,850 * b_{b_p}(470\,\mathrm{nm})\right) + 57.47 \quad (1)$$

($n = 11$; $R^2 = 0.55$; $p < 0.01$; Figure S3 in Supporting Information S1). In situ samples were collected by filtering known volumes of seawater through combusted Whatman GF/F filters, dried at 60°C, and analyzed for POC on a Costech ECS Model 4010 elemental analyzer at the Virginia Institute of Marine Science (Gardner et al., 2000).

2.2. Net Community Production

In assessing POC production and export processes, we grouped the data into continuous five-day increments (1–5 December, 6–10 December, 11–15 December, 16–20 December, 21–25 December 26–30, December, 31 December–4 January, 5–7 January, 8–12 January, 13–17 January, 18–22 January, 23–27 January, 28 January–1

February, and 2–6 February). Five-day increments were chosen because lag time between production and export of organic matter from the euphotic zone is believed to be about 5 days in high latitudes (Laws & Maiti, 2019). To separate the three phases, the period after 5 January was shortened to 3 days; that change was included in the calculations. NCP in the top 100 m was calculated based on a modified version of the equation used by Alkire et al. (2014):

$$\mathrm{NCP}_{100} = \mathrm{PQ} * \left(\int_0^{100} \frac{\partial O_2}{\partial t} - F_{K_z} - F_{\mathrm{Adv}} - \mathrm{ASE}_{\mathrm{ML}} \right) \tag{2}$$

where $\int_0^{100} \frac{\partial \mathrm{O}_2}{\partial t}$ is the change in O_2 concentrations integrated over the top 100 m from Day 1 to 5. The surface 100 m was chosen as our integration depth because it is a commonly used threshold when assessing production-export dynamics (Martin et al., 1987). F_{K_z} is the vertical eddy diffusion flux calculated according to:

$$F_{K_z} = K_Z * \frac{\partial \mathrm{O}_2}{\partial z} \tag{3}$$

where K_Z is vertical diffusivity ($\mathrm{m}^2\ \mathrm{s}^{-1}$), and $\frac{\partial \mathrm{O}_2}{\partial z}$ is change in oxygen concentration in the vertical direction (μmol $\mathrm{kg}^{-1}\ \mathrm{m}^{-2}$). For our K_Z values, we used an estimate previously published from Kaufman et al. (2017) of $10^{-3}\ \mathrm{m}^2\ \mathrm{s}^{-1}$ averaged over the top 200 m. F_{Adv} is advective flux in the longitudinal and latitudinal directions where F_{Adv} is calculated as:

$$F_{\mathrm{Adv}} = \left(u \frac{\partial \mathrm{O}_2}{dx} \right) + \left(v \frac{\partial \mathrm{O}_2}{dy} \right) \tag{4}$$

where u is longitudinal change ($\mathrm{m}\ \mathrm{s}^{-1}$), v is latitudinal change ($\mathrm{m}\ \mathrm{s}^{-1}$), and $\frac{\partial \mathrm{O}_2}{dx}$ and $\frac{\partial \mathrm{O}_2}{dy}$ are change in oxygen concentration in the longitudinal and latitudinal directions (μmol $\mathrm{kg}^{-1}\ \mathrm{m}^{-1}$), respectively. PQ is photosynthetic quotient, and $\mathrm{ASE}_{\mathrm{ML}}$ is air-sea exchange within the mixed layer. A polar-specific photosynthetic quotient of 1.3 was used (Laws, 1991). Air-sea exchange was calculated according to Liang et al. (2013) accounting for bubble injection, using wind speed data ($\mathrm{m}\ \mathrm{s}^{-1}$) and pressure (pascals) data from the National Centers for Environmental Prediction (NCEP) Reanalysis 1 product (2.5° × 2.5° resolution; Kalnay et al., 1996), and gas transfer velocity coefficients from Wanninkhof (1992). When calculating NCP within the mixed layer, calculation of the entrainment flux is necessary, but given all mixed layers on our calculation days are above 100 m, we have omitted this term (Emerson et al., 2008). Additionally, we assume lateral mixing and vertical advection to be negligible compared to the other terms and thus omit it (see Alkire et al., 2014). All variables were converted to units of g $\mathrm{C}\ \mathrm{m}^{-2}\ \mathrm{d}^{-1}$ for final NCP rates.

2.3. Changes in POC Through Time

To assess POC accumulation and removal, we analyzed temporal changes in POC from 0 to 240 m (mean water column depth was ca. 700 m). Because the optical puck was turned off below 250 m, depths below 240 m were not evaluated. Change in POC concentration over time was calculated as:

$$\frac{\partial \mathrm{POC}}{\partial t} = \int_0^{240} \frac{\partial \mathrm{POC}}{\partial t} - F_{\mathrm{Adv}} \tag{5}$$

where $\int_0^{240} \frac{\partial \mathrm{POC}}{\partial t}$ is the change in integrated POC concentration for both Day 1 and 5 (Alkire et al., 2014). F_{Adv} is calculated in the same manner as in Equation 2 but with POC in each equation instead of O_2 (Table S2 in Supporting Information S1). F_{K_z} is omitted from the $\frac{\partial \mathrm{POC}}{\partial t}$ equation because the influence of vertical diffusion on particulate matter is assumed to be negligible (Alkire et al., 2014).

2.4. Calculation of POC Export Potential

We used our NCP rates and $\frac{\partial \mathrm{POC}}{\partial t}$ to investigate the POC export potential through a modified version of the equation of Cassar et al. (2015):

$$\mathrm{Export}_{\mathrm{POC}} = \mathrm{NCP} - \frac{\partial \mathrm{POC}}{\partial t} \tag{6}$$

where $\text{Export}_{\text{POC}}$ is POC export from the surface layer. However, because we are in non-steady state conditions, NCP is not equivalent to export. Therefore, we define $\text{Export}^{*}_{\text{POC}}$ as:

$$\text{Export}^{*}_{\text{POC}} = \text{NCP} - \frac{\partial \text{POC}}{\partial t} \tag{7}$$

where $\text{Export}^{*}_{\text{POC}}$ is POC export potential, a measure of how much POC remains in the surface layer and is exported and/or remineralized over time (Sweeney et al., 2000). Traditionally, $\frac{\partial \text{DOC}}{\partial t}$ would be included in Equation 7, but due to lack of data, dissolved organic carbon (DOC) production is omitted from our estimates.

2.5. Uncertainty

An uncertainty associated with our estimates arises from the in situ calibration of the glider sensors. The Optode was factory calibrated, but because oxygen was not intended to be a key parameter of interest for analysis, no Winkler titration oxygen samples were taken. Given we are using changes in oxygen concentrations for our analysis, discrete oxygen concentrations are not of primary interest, and ∂O_2 estimates are still accurate (B. Y. Queste et al., 2015). However, caution should be taken when analyzing dissolved oxygen concentration trends (Figure 4) as these values may overestimate concentrations given the uncertainty on factory calibrated Optodes can be high (Bittig et al., 2018). In situ POC and fluorescence samples were collected upon glider deployment and recovery and were used to calibrate the Echo Sounder and ECO Triplet Puck (Figures S3 and S4 in Supporting Information S1). Representative relationships were developed, but given the relatively few calibration samples and dynamic nature of the study environment, this presents another source of uncertainty. Additionally, euphotic zone depths were calculated based on chlorophyll concentration (Morel, 1974) rather than photosynthetically active radiation, and as such are likely to be influenced by chlorophyll changes associated with phytoplankton physiology. However, because euphotic zone depths are provided for ecosystem context but not incorporated into our rate calculations, this does not factor in as an uncertainty within our estimates.

Another large source of uncertainty in our estimates of NCP is associated with the air-sea exchange calculation (Naegler et al., 2006). To estimate NCP uncertainty, we used upper (±71%) and lower bound (±34%) uncertainties previously reported for K_z as well as reported uncertainties associated with the bubble parameterization (±7–10%) and Schmidt number (±7–10%) in the air-sea exchange model (Yang et al., 2017). To account for uncertainties associated with the calibration between glider and CTD O_2 measurements, we used the offset at time zero (i.e., the *y*-intercept; Yang et al., 2017) of ±5.5%. We then propagated the individual variable errors to generate one error estimate for the NCP mass balance equation. This approach gave us an uncertainty of ±38.0–73.2% for NCP. We present the average of ±55.6% as the light gray shaded region on Figure 6. The same approach was taken to calculate the uncertainty associated with $\frac{\partial \text{POC}}{\partial t}$ but substituting the offset between glider and CTD O_2 concentrations for POC concentrations, giving an uncertainty of ±12.6%.

As was previously mentioned, the lack of available DOC data constitutes another uncertainty. However, DOC generation during photosynthesis is typically a minor fraction of phytoplankton production during active growth (Carlson et al., 2000; Hansell & Carlson, 1998; Sweeney et al., 2000). Provided that DOC production is low, this parameter is considered a small component of NCP and thus unlikely to influence our estimates (Cassar et al., 2015). However, given the lack of DOC data, the calculated $\text{Export}^{*}_{\text{POC}}$ may be a slight overestimate.

Finally, we are assessing temporal changes outside of a Lagrangian framework. By calculating advective fluxes, we are separating out spatial biases associated with variable water masses (Alkire et al., 2014). However, due to unavoidable microscale variability, some biases may still occur and cause slight over- or underestimations.

3. Results

3.1. POC Concentrations

POC concentrations were relatively low in early December (average of 241 mg C m^{-3} at the surface during Phase 1; Table 1) and showed a typical biological profile, with the greatest vertical decrease from the base of the euphotic zone to 50 m (Figures 2–4). The mean euphotic zone depth derived from chlorophyll concentrations was 19.8 m during this period; average euphotic zone integrated chlorophyll was 80.6 mg Chl a m^{-3} (Figure S5 in Supporting Information S1). Concentrations of POC in the upper 150 m always decreased with depth (Figures 3

Table 1
Mean Particulate Organic Carbon Concentrations (POC; mg C m^{-3}) From 0–240 m in All Phases

Phase	I	II	III
POC at 0 m	241	347	235
POC at 25 m	154	267	233
POC at 50 m	105	202	194
POC at 75 m	90.8	160	153
POC at 100 m	80. 9	125	108
POC at 150 m	67.0	69.1	80.9
POC at 200 m	57.1	49.7	67.2
POC at 240 m	53.7	56.4	63.8
Z_{eu} (m)	19.8	29.6	56.7
MLD (m)	31.9	35.1	46.7

Note. Average euphotic zone depths (Z_{eu}) and mixed layer depths (MLD) for each phase are also listed.

and 4). Patterns of POC changes were consistent in the upper 100 m but were dampened and temporally uncoupled below 150 m. Surface concentrations in the upper 50 m increased due to phytoplankton production, and nearly doubled between Phases I and II (Figures 3 and 4). Similarly, POC concentrations at 100 m increased by 62% over the same period. Concentrations at depth (≥150 m) during Phase I were nearly invariant and low (ca. 55 mg C m^{-3}), but increased slightly during Phase II, and reached a maximum in Phase III before declining (Figures 3 and 4). The greatest change in POC concentrations occurred between 100 and 150 m, where they decreased by 7%–46% through time (Figure 4). The increases at 150, 200, and 240 m from the beginning of Phase I to their maximum represented increases of 38%, 32%, and 26%, respectively. During Phase III, the vertical profiles were less uniform and exhibited greater variability from the euphotic zone through 150 m.

Abrupt changes to POC concentrations (e.g., 10 and 29 December, 18, 21, and 25 January, and 3 February) corresponded to perturbation events (i.e., periods of enhanced wind speeds (>10 m s^{-1} and rapid mixed layer deepening (>70 m); Figures 3–5). Average mixed layer depths were 32, 35, and 47 m for Phases I, II, and III, respectively (Table 1), but were highly variable (standard deviations were 13.4, 22.6, and 23.5 m for Phases I, II, and III, respectively) during these high wind events. Abrupt changes in mixed layer depth appear temporally uncoupled to substantial changes in temperature and salinity (Figure S6 in Supporting Information S1), suggesting these changes are unlikely caused by heat loss or gain. These increased mixed layers in Phase III corresponded to increased surface to 100 m POC concentration variability.

3.2. Net Community Production

NCP varied considerably over the course of the bloom, as the rates ranged from −3.79 to 4.88 g C m^{-2} d^{-1}; the mean for the entire study was 0.05 ± 2.75 g C m^{-2} d^{-1} (Figure 6). NCP showed substantial variability within and across phases, frequently changing between net heterotrophy and net autotrophy (Figure 6). Highest production occurred within Phase II with an average NCP rate of 1.66 g C m^{-2} d^{-1}. Phases I and III average NCP rates were −1.53 and −0.50 g C m^{-2} d^{-1}, respectively (Figure 6). Initial NCP from 1 December to 5 December was low before a temporary increase by 10 December, followed by a substantial decline (>−3 g C m^{-2} d^{-1}) that continued for the rest of Phase I. Phase II rates of NCP were consistently higher (on average 3.19 g C m^{-2} d^{-1}) than Phase I rates. Maximum rates of NCP occurred from 16 December to 20 December, immediately before the period of maximum POC concentrations. Phase III rates of NCP showed a significant decline from Phase II rates (−2.16 g

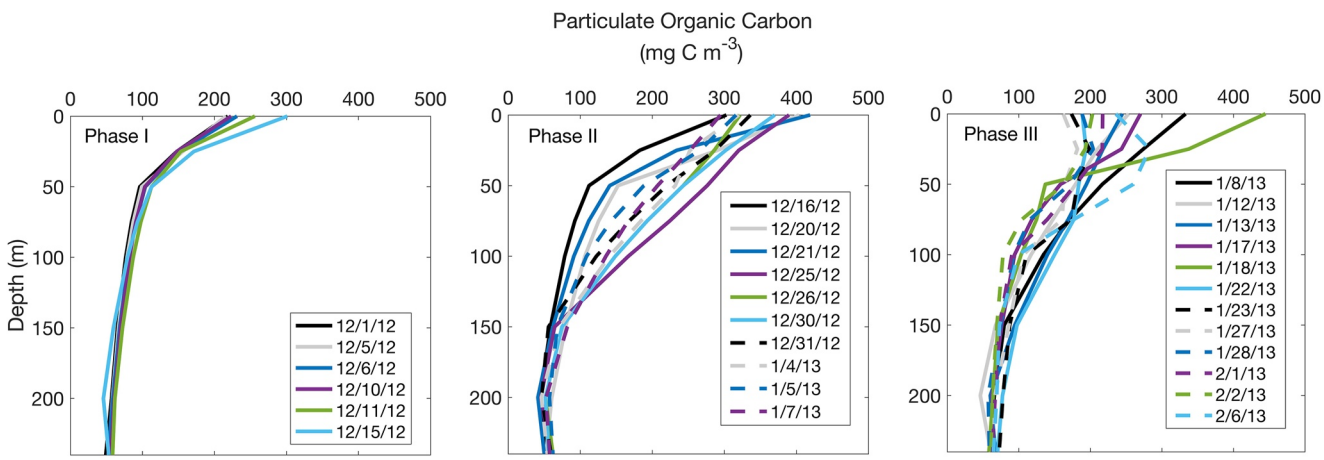

Figure 2. Vertical particulate organic carbon concentrations (mg C m^{-3}) in Phase I, Phase II, and Phase 3. Profiles were calculated by taking the average concentration at 0, 25, 50, 75, 100, 150, 200, and 240 m from all glider up- and down-casts during each day.

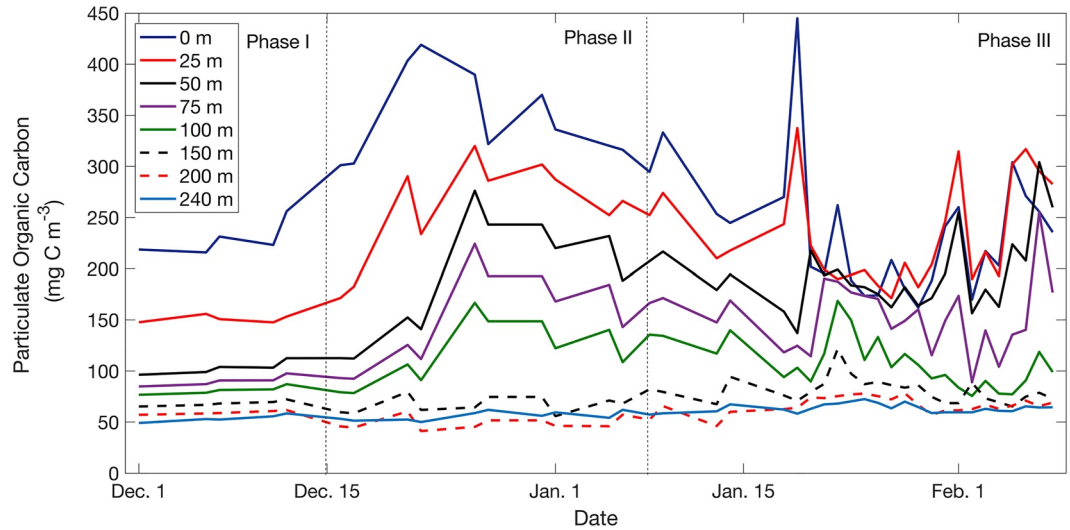

Figure 3. Discrete daily particulate organic matter concentrations (mg C m^{-3}) of a given depth from 1 December to 6 February. Dashed gray lines indicate the phase dates. Concentrations from all of the glider dives on a given day were averaged into one value per depth per day.

C m^{-2} d^{-1}) and had the greatest variability, ranging from −3.79–4.23 g C m^{-2} d^{-1}. The 1–17 January rate was the lowest NCP of the entire period and resulted from a steady decrease in biological oxygen concentrations (−0.41 mol O_2 m^{-2} d^{-1}) from 8 January to 17 January (Figure 4a). The high degree of variability over the course of the bloom is consistent with what we expected in this dynamic, non-steady state system.

Air sea-exchange drove substantial fluctuations in NCP; large declines in NCP are associated with high winds (>5 m s^{-1}, Figure 5) and substantial changes in mixed layer depth. Estimated air-sea exchanges ranged from −0.02 to 0.09 mol O_2 m^{-2} d^{-1} and averaged 0.01 ± 0.03 mol O_2 m^{-2} d^{-1} (or averaged 0.05 ± 0.24 g C m^{-2} d^{-1}; Figure 7; Table S1 in Supporting Information S1). The large and apparently continuous decline in NCP at the end of Phase III was driven by increased winds and increased frequency of strong events (18, 21, and 25 January).

Advective fluxes (F_{Adv}) were not negligible, ranging from −0.02 to 0.01 mol O_2 m^{-2} d^{-1} (−0.21 to 0.11 g C m^{-2} d^{-1}) over the course of the bloom, with highest values measured during Phase II (Figure 7; Table S1 in Supporting Information S1). Average F_{K_z} were comparable to F_{Adv}, ranging from −0.01 to 0.01 mol O_2 m^{-2} d^{-1} (−0.12 to 0.11 g C m^{-2} d^{-1}; Figure 7; Table S1 in Supporting Information S1). The changes induced by physical transport mechanisms were highly variable but on average were still 1–2 orders of magnitude less than those of total dissolved oxygen change, suggesting that the majority of oxygen dynamics within the Ross Sea productive period were driven by biological processes.

3.3. $\frac{\partial POC}{\partial t}$

Throughout the bloom $\frac{\partial POC}{\partial t}$ ranged from −1.61 to 2.84 g C m^{-2} d^{-1} and averaged 0.22 ± 1.24 g C m^{-2} d^{-1} (Figure 6). Phase averages were −0.10, 0.93, and −0.22 g C m^{-2} d^{-1} for Phases I, II, and III, respectively (Figure 6). In this context, negative $\frac{\partial POC}{\partial t}$ indicates an increase in POC concentrations due to substantial NCP within the upper 240 m from Day 1 to Day 5. On average POC accumulated within the water column during Phase I and Phase III, whereas POC decreased during Phase II. Highest rates of $\frac{\partial POC}{\partial t}$ coincided with the periods of highest POC concentrations in the upper 100 m. Despite substantial variability, the average $\frac{\partial POC}{\partial t}$ remained positive, that is, average POC was decreasing.

Highest rates of $\frac{\partial POC}{\partial t}$ in the top 240 m were 2.84 g C m^{-2} d^{-1} and were observed 5 days after the highest NCP during 16–20 December, suggesting a slight temporal uncoupling between the two (Figure 6). Paired *t*-tests between NCP and $\frac{\partial POC}{\partial t}$ per phase and over the course of the bloom yielded *p*-values all greater than >0.1 suggesting that production and export dynamics are not significantly correlated. These processes are coupled ecologically, but are likely statistically uncoupled due to a variety of confounding factors (small numbers of data points

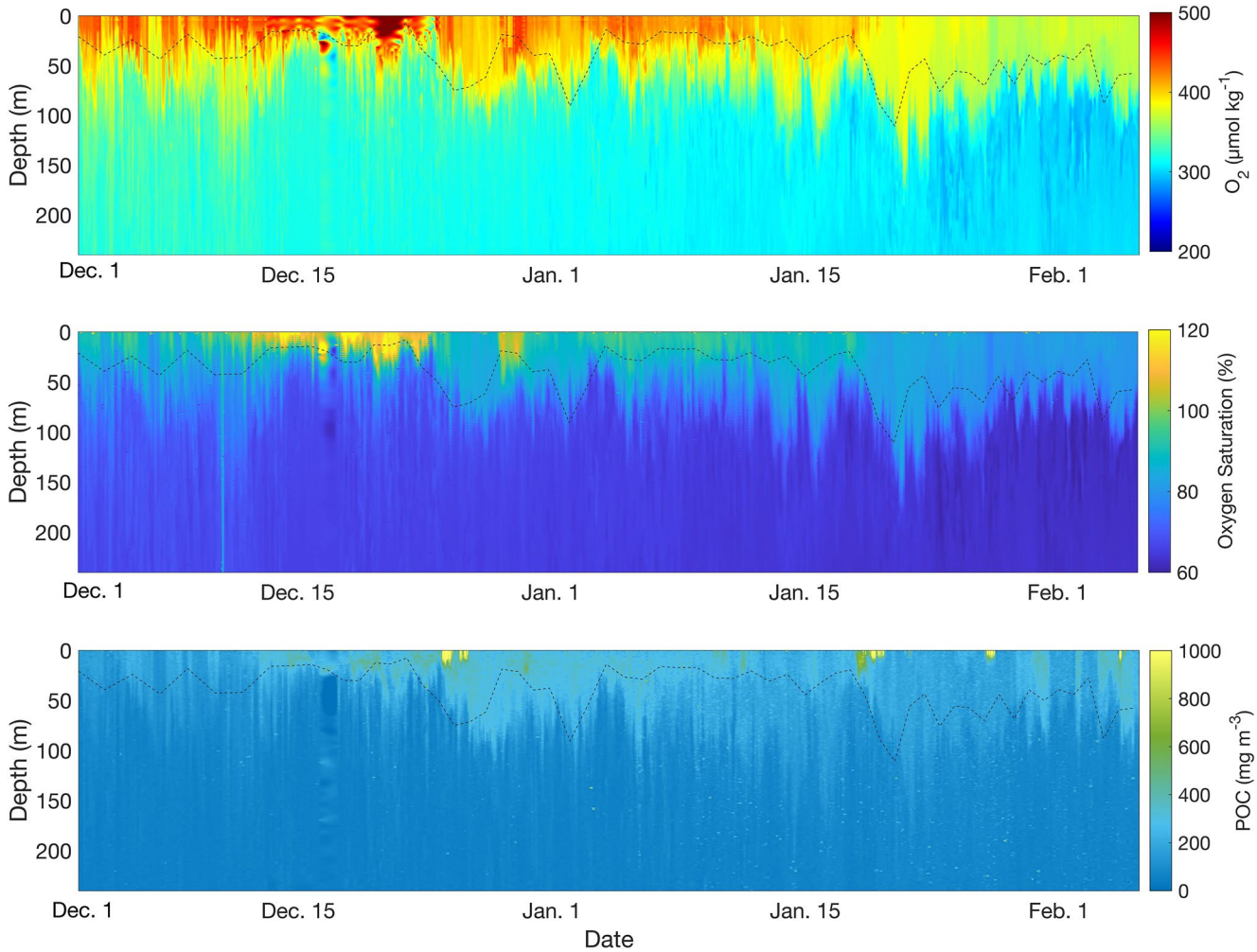

Figure 4. Temporal patterns of dissolved oxygen concentrations (µmol kg^{-1}), oxygen saturation (%), and particulate organic carbon concentrations (mg m^{-3}) in the upper 240 m from the glider transect. Dashed lines indicate mixed layer depths.

(14 per NCP and $\frac{\partial POC}{\partial t}$, respectively), changing remineralization length scales for *Phaeocystis* vs. diatoms, and varying levels of biomass in the surface). Additionally, the limited duration over which we evaluate the parameters likely influenced the statistical relationships and thus underscores the need to evaluate production and export dynamics on complete seasonal or annual timescales.

3.4. POC Export Potential

The average $Export^{*}_{POC}$ was −0.17 g C m^{-2} d^{-1} (Figure 6). Trends in $Export^{*}_{POC}$ were consistent with trends in NCP, with $Export^{*}_{POC}$ being high (0.73 g C m^{-2} d^{-1}) during Phase II, lower during Phase III (−0.28 g C m^{-2} d^{-1}), and lowest during Phase I (−1.43 g C m^{-2} d^{-1}; Figure 6). However, peak $Export^{*}_{POC}$ occurred during Phase III between 18 January and 22 January when NCP has high and $\frac{\partial POC}{\partial t}$ was low. $Export^{*}_{POC}$ was highly variable (similar to NCP), with values ranging from −2.70 to 4.57 g C m^{-2} d^{-1} (Figure 6). Negative $Export^{*}_{POC}$ is driven by negative NCP (i.e., a decrease in production due to physical forcing or high community respiration rates), and can result from physical or biological changes in the upper 100 m. The high percentage (>60%) of periods with negative $Export^{*}_{POC}$ likely results from highly variable NCP rates and temporal decoupling between NCP and $\frac{\partial POC}{\partial t}$ during temporary periods of net heterotrophy.

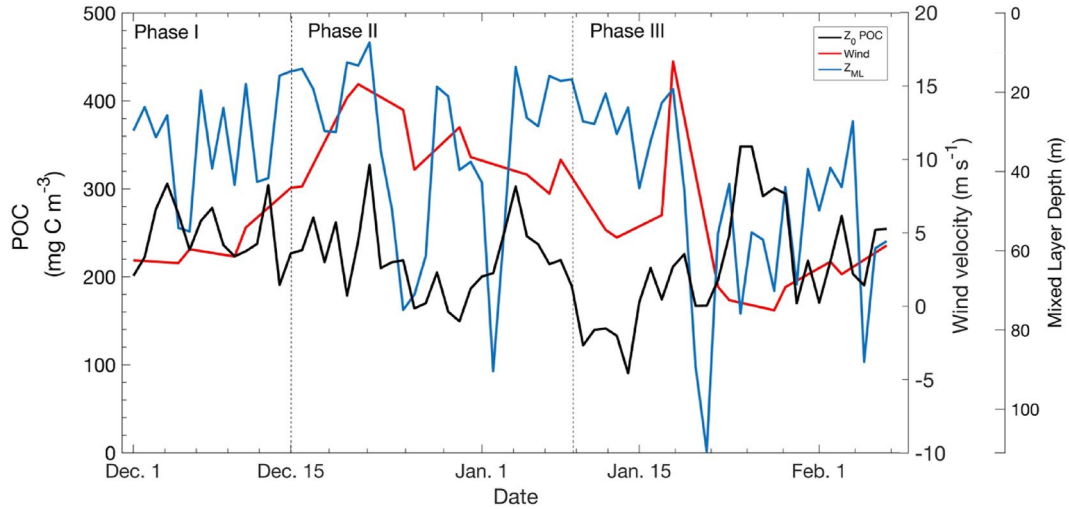

Figure 5. Daily surface particulate organic carbon concentrations (mg C m^{-3}; black line), average wind speeds (m s^{-1}; red line), and mixed layer depths (m; blue line) from 1 December to 6 February. Wind speed data are from the National Centers for Environmental Prediction Reanalysis 1 product (Kalnay et al., 1996). Dashed gray lines indicate the phase.

4. Discussion

While the dynamics of the Ross Sea annual productive period have been well studied (Schine et al., 2015; Smith et al., 2000, 2013), logistical challenges have prevented most fine-scale studies, although a few high-resolution analyses have been completed (Hales & Takahashi, 2004). This study represents the highest resolution analysis of POC distributions within the Ross Sea austral spring and summer to date. Our POC profiles demonstrate the progression of the annual productive period (Figures 2 and 3); the accumulation (Phase I), maxima (Phase II), and its decline (Phase III) likely correspond to the progression of the spring *Phaeocystis* bloom, as well as the subsequent export of organic material from the surface to deeper waters (Figure 2; Jones & Smith, 2017; Smith et al., 2000). The change from an exponential decline below the mixed layer in Phase I to the decreases in Phases II and III is a function of the large POC changes below 50 m (Figure 2). The increase in POC concentrations at 50 and 100 m from Phase I to Phase II was substantial (ca. 100%–150% more in Phase I than in II; Table 1), and almost certainly results from a large mass of sinking particles from the euphotic zone. The profiles in the beginning of Phase III exhibit the same general shape as profiles in Phase II, but they show increased variability in the upper 100 m concentrations and a decoupling of concentrations between the surface to upper 100 m (Figure 2). Concentrations also decrease from 100 to 150 m over time, but return to consistently low values at 240 m by late Phase III. We suggest that the decrease in 0–25 m POC concentrations during this period (13 January 13–1 February) likely reflected a period of increased, wind-driven, vertical mixing that induced export of water from the surface, thus enhancing POC export. The mechanism for initiating increased export is unclear, but it is possible that an increased number of particle interactions in a turbulent environment led to the formation of larger, more rapidly sinking aggregates (Burd & Jackson, 2009).

Throughout our study, the 200–240 m average POC concentrations slowly increased through time and reached maximum values in Phase III (Table 1). This suggests that from 50–200 m $\frac{\partial \mathrm{POC}}{\partial t}$ occurred at a faster rate than those at 240 m. Through a variety of techniques, previous studies have suggested substantial remineralization of *P. antarctica* in the upper 100–150 m, consistent with our findings (Asper & Smith, 2019; Jones & Smith, 2017; Reigstad & Wassmann, 2007). Conversely, diatom-associated carbon is thought to be remineralized less rapidly, since the carbon associated with the siliceous tests may sink more rapidly than does non-silica associated organic material and therefore reach greater depths (Twinning et al., 2014), although this may not be universally true (Yasuda et al., 2016).

There was a slight increase in POC concentrations (~10 mg C m^{-2} d^{-1}) from 200 to 240 m (Figure 3, Table 1). During Phase III the average POC in the upper 100 m decreased (Figure 3), coinciding with substantial increases in POC at 150, 200, and 240 m (11, 18, and 21 mg C m^{-2}; Table 1) and decreases in oxygen concentrations and

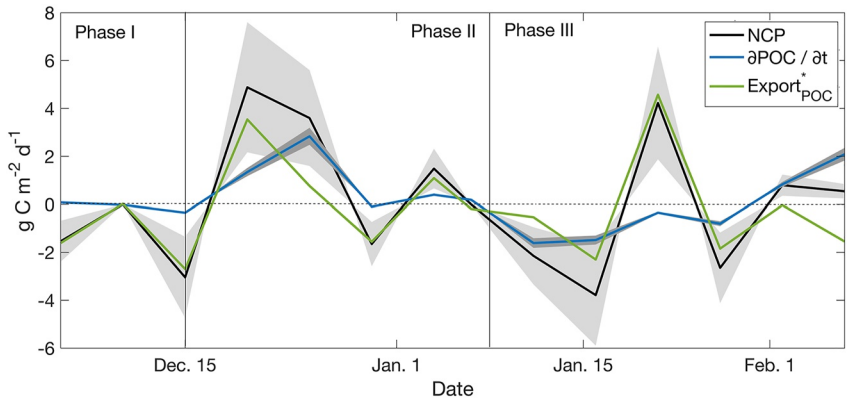

Figure 6. Temporal patterns of net community production (NCP; mg C m^{-2} d^{-1}), $\frac{\partial POC}{\partial t}$ (mg C m^{-2} d^{-1}), and particulate organic carbon export potential ($Export^{*}_{POC}$; mg C m^{-2} d^{-1}) calculated over five day increments from 1 December to 6 February. Phases are designated with dashed lines. Uncertainty estimates are represented in light gray for NCP and dark gray for $\frac{\partial POC}{\partial t}$.

saturation in the upper 100 m (Figure 4). The changes in POC and oxygen concentrations suggest an increase in heterotrophic remineralization of POC in the upper 100 m. Ducklow et al. (2001) found that bacterial biomass was greatest during late January throughout the upper 300 m of the water column, and Caron et al. (2000) also found that microzooplankton abundance reached a maximum at the same time. The seasonal patterns of both of

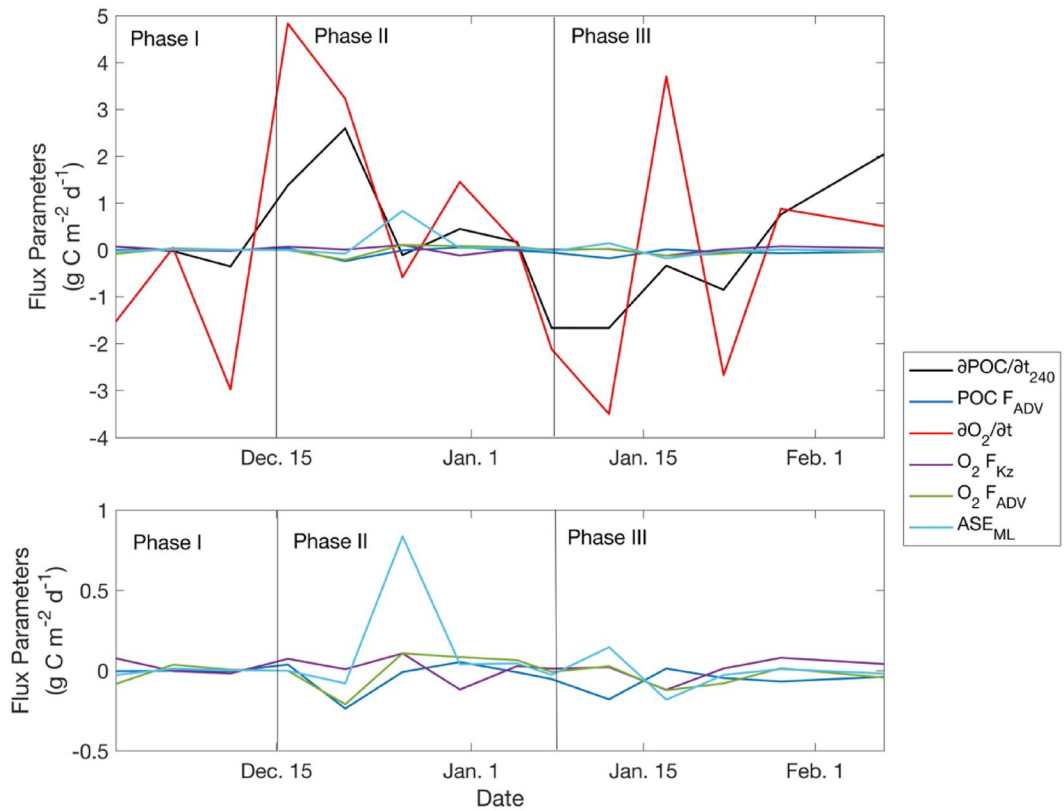

Figure 7. Temporal patterns of the different flux parameters (in units of g C m^{-2} d^{-1}) that compose the $\frac{\partial POC}{\partial t}$ and net community production calculations calculated over five day increments from 1 December to 6 February. The top panel includes all parameters: $\int_0^{240} \frac{\partial POC}{\partial t}$ (labeled as $\frac{\partial POC}{\partial t}_{240}$), advective flux ($F_{Adv}$) for POC, $\int_0^{100} \frac{\partial O_2}{\partial t}$ (labeled as $\frac{\partial O_2}{\partial t}$), vertical eddy diffusion flux (F_{K_z}) for O_2, advective flux (F_{Adv}) for O_2, and air-sea exchange (ASE_{ML}). $\int_0^{240} \frac{\partial POC}{\partial t}$ and $\int_0^{100} \frac{\partial O_2}{\partial t}$ are removed in the bottom panel to allow for trends associated with the other fluxes to be more apparent on a smaller scale. Vertical lines indicate different phases.

these heterotrophic assemblages are consistent with the late summer decreases in POC that we observed in the upper 100 m, which must have resulted from heterotrophic processes.

The Ross Sea is a region of substantial primary production, with annual rates exceeding 200 g C m^{-2} (Smith & Kaufman, 2018; Smith et al., 2006). Estimating rates of NCP are crucial in assessing system dynamics following enhanced productivity as well as POC export potential. Previous studies have calculated NCP rates through carbon budgets (Bates et al., 1998; Sweeney et al., 2000), nutrient deficits (Smith, Shields, et al., 2011; Sweeney et al., 2000), and O_2/Ar ratios (Long et al., 2011). Previous NCP estimates are highly variable, ranging from 0.13 g C m^{-2} d^{-1} to 96 g C m^{-2} over the productive season (Long et al., 2011; Smith et al., 2006). These rates are comparable, albeit slightly lower than our values and may be due to interannual variability, methodological differences (including longer integration times associated with oxygen-based productivity estimates; Cassar et al., 2009), and/or lower resolution sampling. Previously reported ratios of NCP: primary production suggest low rates of community respiration and substantial particulate matter accumulation (i.e., export potential) in the upper water column, consistent with our findings (Long et al., 2011; Smith et al., 2006; Sweeney et al., 2000). Substantial biomass retention may suggest that loss processes are highly variable in time (Smith et al., 2006), and during the seasonally productive period, rates of production and accumulation greatly exceed rates of loss processes.

Export has also been known to be linked to surface phytoplankton composition and physiology (Bach et al., 2016; Burd & Jackson, 2009; Guidi et al., 2009). The southern Ross Sea is known to support a spring bloom of *P. antarctica*, which generally is followed by the growth of diatoms (Smith, Ainley, et al., 2014). This pattern is reflected in the POC:chl ratios (Kaufman et al., 2014; Smith & Kaufman, 2018); that is, the initial *P. antarctica* bloom has "normal" values, but diatoms have greatly elevated ratios as an adaptation to growth in an iron-limited environment (Ryan-Keogh & Smith, 2021). Our glider data confirm this pattern (Figures S5 and S7 in Supporting Information S1), and from this we infer that *Phaeocystis* dominated Phases I and II and diatoms became much more prevalent in Phase III. The trends observed during the *Phaeocystis*-dominated portion of the bloom may result from unique and contrasting export dynamics associated with the different morphotypes of *Phaeocystis*. Single *Phaeocystis* colonies and ghost colonies can sink quickly while single cells likely do not sink (Asper & Smith, 2019; DiTullio et al., 2000). Colonial forms appear labile and subject to substantial bacterial remineralization in the upper 300 m (Asper & Smith, 2019). Additionally, the decrease in biological oxygen concentrations coincident with the shift from the *Phaeocystis* to diatom dominated assemblage may suggest active remineralization of the *Phaeocystis*.

The presumed change in taxonomic composition corresponds to a decoupling between $\frac{\partial POC}{\partial t}$ and NCP from Phase II to III. In Phases I and II, changes in $\frac{\partial POC}{\partial t}$ appears to lag changes in NCP slightly, consistent with what has been observed in sediment trap data and model studies (Figure 6; Kaufman et al., 2017; Smith, Shields, et al., 2011). However, when composition shifts to a predominance of diatoms in Phase III, changes in $\frac{\partial POC}{\partial t}$ appear to lag changes in NCP by a much longer period (~28–50 days; Smith & Dunbar, 1998; Smith, Shields, et al., 2011). The variability we observed in $\frac{\partial POC}{\partial t}$ during Phase III, particularly from 100 to 200 m, may have resulted from the spatially variable growth of diatoms and changes to sinking and remineralization length scales, resulting in a more complex pattern of POC concentration change. While assessing the role of the different taxa on carbon export is outside the realm of this study, the potential influence of diatoms presents interesting implications for future changes to the Ross Sea biological pump, given that diatom populations may increase in coming decades (Kaufman et al., 2017). Overall, taxonomic composition appears to be a dominant factor in regulating export dynamics, and the peak $\frac{\partial POC}{\partial t}$ during the period of presumed *Phaeocystis* dominance would lend support to challenges to the theory that large, dense cells (such as diatoms) dominate export processes (Cassar et al., 2015; S. A. Henson et al., 2021; Juranek et al., 2020).

Higher export rates can result from zooplankton ingestion of phytoplankton and production of fecal pellets (as well as the release of partially ingested particles via sloppy feeding; Steinberg et al., 2008), and zooplankton grazing is strongly regulated by phytoplankton composition. In the Ross Sea, *P. antarctica* is generally considered to be unpalatable and avoided by most mesozooplankton (Smith, Ainley, et al., 2014), although in situ grazing estimates are lacking. Microzooplankton herbivory on colonial *P. antarctica* is nearly zero (Caron et al., 2000). Mesozooplankton abundance and grazing in the Ross Sea are considered to have minor impacts on phytoplankton biomass (Smith, Ainley, et al., 2014), although sediment traps have recorded a substantial number of fecal pellets late in the summer (Dunbar et al., 1998; Smith, Shields, et al., 2011). Rapidly sinking particles would

rarely be observed in glider POC profiles, and based on our carbon budgets, likely do not constitute a major component of POC export on a seasonal basis, a conclusion generalized for much of the ocean (Turner, 2002). Export also includes passive sinking of intact cells and of aggregates that sink more rapidly than solitary cells (Asper & Smith, 1999). Passively sinking senescent *P. antarctica* colonies likely are a significant component of our rates of $\frac{\partial \mathrm{POC}}{\partial t}$, especially in the upper 150 m during Phases I and II. Aggregates also likely contribute substantially to the $\frac{\partial \mathrm{POC}}{\partial t}$, as aggregate POC accounted for ca. 20% of the total POC in the southern Ross Sea (Asper & Smith, 1999, 2019).

Previous studies have calculated carbon export potential in the Ross Sea during austral summer (Hansell & Carlson, 1998; Sweeney et al., 2000). Sweeney et al. (2000) calculated a total carbon export potential of 81% of NCP. Various other studies have calculated carbon export in the Ross Sea through direct-sampling methods, such as sediment traps (Collier et al., 2000; Dunbar et al., 1998; Langone et al., 1997; Smith, Shields, et al., 2011) and thorium measurements (Cochran et al., 2000). Significant methodological differences exist among these and autonomous assets and have led to export rates calculated via a mass balance being substantially larger than those estimated from sediment traps. Given our study ended in early February and the known lags between production and export, this study misses the final diatom reduction, making calculations of the ratio of seasonal POC export potential to NCP difficult. However, a coupling between temporal NCP and POC export potential dynamics and substantial $\frac{\partial \mathrm{POC}}{\partial t}$ over the seasonal period is evident. Thus, high NCP and high POC export potential suggest that overtime, total net $\frac{\partial \mathrm{POC}}{\partial t}$ will be large.

The variable but high NCP, high POC export potential, and the substantial decline in POC concentrations from the upper 100–240 m we derived suggest low biological carbon pump efficiency, similar to previous estimates from other regions of the Southern Ocean (Buesseler et al., 2020; S. Henson et al., 2019). Sweeney et al. (2000) found that only 27% of NCP was exported below 100 m, although substantial variability was also present (±25%). These results are consistent with the substantial upper water column remineralization we observe, underscoring the episodic nature of carbon export dynamics within the Ross Sea and how export pulses can be unresolved when calculating seasonal (or even short-term) averages. Therefore, in highly dynamic environments like the Southern Ocean, it is particularly important to assess NCP, $\frac{\partial \mathrm{POC}}{\partial t}$, and POC export potential through temporal patterns rather than by seasonal averages.

One advantage of estimating POC dynamics from glider data is that it allows us to estimate changes in various portions of the water column instead of those for the entire water column. PAR and fluorescence sensors on gliders also allow the calculation of specific euphotic zone depths and mixed layer depths, enabling better understanding of the potential processes influencing export potential than are generally possible with fixed measurements (Buesseler et al., 2020). Our results indicate that POC removal processes (i.e., remineralization, flux to depth) within the water column are non-uniform in time. This is likely biologically driven because primary production, microbial remineralization, and taxonomic controls on sinking rates all vary in time.

The overall, $\frac{\partial \mathrm{POC}}{\partial t}$ from 0 to 240 m ranges from −1.61 to 2.84 g C m^{-2} d^{-1}, and $\mathrm{Export}^{*}_{\mathrm{POC}}$ ranges from −2.70 to 4.57 g C m^{-2} d^{-1} (Figure 6). The December–February period is responsible for 90% of Ross Sea annual primary production, although export of POC may be delayed in time (Sweeney et al., 2000). Our high $\mathrm{Export}^{*}_{\mathrm{POC}}$ relative to NCP suggests active remineralization but an overall accumulation of POC. However, export and $\mathrm{Export}^{*}_{\mathrm{POC}}$ appear to be slightly decoupled but temporally dependent; evidence of high export efficiency to depths below 200 m in the Ross Sea in the early autumn have been reported (February–March; DeJong et al., 2017). Although substantial changes in primary productivity and assemblage composition make it necessary to consider the Ross Sea phytoplankton bloom dynamics dependent temporal trends, the high rates of NCP and accumulation of POC within the upper water column throughout the productive period reinforce the conclusion that the Ross Sea plays an important role in Southern Ocean and global carbon cycling.

In addition to the roles taxonomy and trophic interactions play in controlling NCP, $\frac{\partial \mathrm{POC}}{\partial t}$, and $\mathrm{Export}^{*}_{\mathrm{POC}}$, the variable mixed layer depth appears to be a substantial control on production and export dynamics. Previous studies have highlighted the need to consider seasonal fluctuations of the mixed layer and the redistribution of organic matter throughout the water column, particularly at high latitudes (Dall'Olmo et al., 2016). Our results support these findings as substantial declines in NCP, and subsequently $\frac{\partial \mathrm{POC}}{\partial t}$ and $\mathrm{Export}^{*}_{\mathrm{POC}}$, occur during the periods 21–25 December to 26–30 December and 18–22 January to 23–27 January when mixed layers deepen dramatically (−71.8 and −91.5 m) over short time periods (approximately 4–6 days; Figure 5). During these periods,

air-sea exchanges also change substantially due to wind impacts on the in- and out-gassing of oxygen (Table S1 in Supporting Information S1). Highly variable mixed layer depths have been reported for the Southern Ocean (Ryan-Keogh & Smith, 2021; Salle et al., 2010; Smith et al., 2013) and the relationship between mixed layer depth, NCP, $\frac{\partial POC}{\partial t}$, and $Export^{*}_{POC}$ we observed is likely representative of typical biophysical dynamics in the Southern Ocean during the spring season.

The role of this "mixed layer pump" is an important but poorly characterized control on export in the biological carbon pump. Our results highlight the importance of high-wind events on mixed layer depths and air-sea exchange and consequently, the impacts on POC distributions and NCP. Deep and fluctuating mixed layers occur in other regions associated with high primary production such as the North Atlantic and Northwest Pacific (Dall'Olmo et al., 2016) and thus, the impacts of the mixed layer pump we found are comparable to those in other climatically important regions. However, in other systems wind forcing has been shown to enhance pulses of POC export, a process we did not observe (Lacour et al., 2019). Further investigation into the relationship between mixing dynamics and export processes, particularly utilizing high resolution sampling methods such as gliders to resolve changes on short time scales, is warranted.

5. Conclusions

Ross Sea POC concentrations and export potential to depth show substantial vertical and temporal changes due to shifts in surface POC concentrations, primary production, phytoplankton composition, and rates of biological remineralization. While more research is needed to fully evaluate the influence of each of these factors on export dynamics, our results represent an important step in quantifying Ross Sea POC change and export potential and their biological and physical controls. Our findings highlight the benefits that autonomous vehicles provide in enhancing observational capabilities, leading to a more comprehensive understanding of dynamics within temporally and vertically resolved frameworks as well as the role of lag times between processes when observed over finer scales. Further investigations on similar space and time scales are necessary to more accurately understand and model the biological pump and carbon cycle in other parts of the Southern Ocean, and to assess changes that will occur under future climate scenarios.

Data Availability Statement

All data is publicly available at the Biological and Chemical Oceanography Data Management Office: https://www.bco-dmo.org/dataset/568868.

Acknowledgments
This work was funded by a US National Science Foundation grant (ANT 1142174 to WOS) and PRC awards No. 41876228 and 41941008. We thank Dr. Rachel Stanley for helpful NCP discussions and Dr. Nathan Briggs for comments on an earlier version of this paper.

References

Alkire, M. B., Lee, C., D'Asaro, E., Perry, M. J., Briggs, N., Cetinic, I., & Gray, A. (2014). Net community production and export from Seaglider measurements in the North Atlantic after the spring bloom. *Journal of Geophysical Research: Oceans*, *119*(9), 6121–6139. https://doi.org/10.1002/2014JC010105

Arrigo, K. R., & van Dijken, G. L. (2003). Phytoplankton dynamics within 37 Antarctic coastal polynya systems. *Journal of Geophysical Research*, *108*(C8), 3271. https://doi.org/10.1029/2002JC001739

Arrigo, K. R., & van Dijken, G. L. (2004). Annual changes in sea-ice, chlorophyll a, and primary production in the Ross Sea, Antarctica. *Deep-Sea Research II*, *51*(1–3), 117–138. https://doi.org/10.1016/j.dsr2.2003.04.003

Arrigo, K. R., van Dijken, G. L., & Long, M. (2008). Coastal Southern Ocean: A strong anthropogenic CO_2 sink. *Geophysical Research Letters*, *35*(21), L21602. https://doi.org/10.1029/2008GL035624

Asper, V., & Smith, W. O., Jr. (1999). Particle fluxes during austral spring and summer in the southern Ross Sea, Antarctica. *Journal of Geophysical Research*, *15*(C3), 5345–5359. https://doi.org/10.1029/1998JC900067

Asper, V., & Smith, W. O., Jr. (2019). Variations in the abundance and distribution of aggregates in the Ross Sea, Antarctica. *Elementa Science of the Anthropocene*, *7*, 23. https://doi.org/10.1525/elementa.355

Bach, L. T., Boxhammer, T., Larsen, A., Hildebrandt, N., Schulz, K. G., & Riebesell, U. (2016). Influence of plankton community structure on the sinking velocity of marine aggregates. *Global Biogeochemical Cycles*, *30*(8), 1145–1165. https://doi.org/10.1002/2016GB005372

Bates, N. R., Hansell, D. S., Carlson, C. A., & Gordon, L. I. (1998). Distribution of CO_2 species, estimates of net community production and air-sea CO_2 exchanges in the Ross Sea polynya. *Journal of Geophysical Research*, *103*(C2), 2883–2896. https://doi.org/10.1029/97jc02473

Bittig, H. C., Kortzinger, A., Neill, C., van Ooijen, E., Plant, J. N., Hahn, J., et al. (2018). Oxygen optode sensors: Principle, characterization, calibration, and application in the ocean. *Frontiers in Marine Science*, *4*, 429. https://doi.org/10.3389/fmars.2017.00429

Boss, E., & Pegau, W. S. (2001). Relationship of light scattering at an angle in the backward direction to the backscattering coefficient. *Applied Optics*, *40*(30), 5503–5507. https://doi.org/10.1364/AO.40.005503

Buesseler, K. O., & Boyd, P. W. (2009). Shedding light on processes that control particle export and flux attenuation in the twilight zone of the open ocean. *Limnology and Oceanography*, *54*(4), 1210–1232. https://doi.org/10.4319/lo.2009.54.4.1210

Buesseler, K. O., Boyd, P. W., Black, E. E., & Siegel, D. A. (2020). Metrics that matter for assessing the ocean biological carbon pump. *Proceedings of the National Academy of Sciences of the United States of America*, *117*(18), 9679–9687. https://doi.org/10.1073/pnas.1918114117

Burd, A. B., & Jackson, G. A. (2009). Particle aggregation. *Annual Review of Marine Science*, *1*, 65–90. https://doi.org/10.1146/annurev.marine.010908.163904

Carlson, C. A., Hansell, D. A., Peltzer, E. T., & Smith, W. O., Jr. (2000). Stocks ad dynamics of dissolved and particulate organic matter in the southern Ross Sea, Antarctica. *Deep Sea Research II*, *47*(15–16), 3201–3225. https://doi.org/10.1016/S0967-0645(00)00065-5

Caron, D. A., Dennett, M. R., Lonsdale, D. J., Moran, D. M., & Shalapyonok, L. (2000). Microzooplankton herbivory in the Ross Sea, Antarctica. *Deep-Sea Research II*, *47*(15–16), 3249–3272. https://doi.org/10.1016/S0967-0645(00)00067-9

Cassar, N., Barnett, B. A., Bender, M. L., Kaiser, J., Hamme, R. C., & Tilbrook, B. (2009). Continuous high-frequency dissolved O_2/Ar measurements by equilibrator inlet mass spectrometry. *Analytical Chemistry*, *81*(5), 1855–1864. https://doi.org/10.1021/ac802300u

Cassar, N., Wright, S. W., Thomson, P. G., Trull, T. W., Westwood, K. J., de Salas, M., et al. (2015). The relation of mixed-layer net community production to phytoplankton community composition in the Southern Ocean. *Global Biogeochemical Cycles*, *29*(4), 446–462. https://doi.org/10.1002/2014GB004936

Cochran, J. K., Buesseler, K. O., Bacon, M. P., Wang, H. W., Hirschberg, D. J., Ball, L., et al. (2000). Short-lived thorium isotopes (^{234}Th, ^{228}Th) as indicators of POC export and particle cycling in the Ross Sea, Southern Ocean. *Deep-Sea Research II*, *47*(15–16), 3451–3490. https://doi.org/10.1016/S0967-0645(00)00075-8

Collier, R., Dymond, J., Honjo, S., Manganini, S., Francois, R., & Dunbar, R. (2000). The vertical flux of biogenic and lithogenic material in the Ross Sea: Moored sediment trap observations 1996-1998. *Deep-Sea Research II*, *47*(15–16), 3491–3520. https://doi.org/10.1016/S0967-0645(00)00076-X

Dall'Olmo, G., Dingle, J., Polimene, L., Brewin, R. J. W., & Claustre, H. (2016). Substantial energy input to the mesopelagic ecosystem from the seasonal mixed-layer pump. *Nature Geoscience*, *9*(11), 820–823. https://doi.org/10.1038/NGEO2818

DeJong, H. B., Dunbar, R. B., Koweek, D. A., Mucciarone, D. A., Bercovici, S. K., & Hansell, D. A. (2017). Net community production and carbon export during the late summer in the Ross Sea, Antarctica. *Global Biogeochemical Cycles*, *31*(3), 473–491. https://doi.org/10.1002/2016GB005417

DiTullio, G. R., Grebmeier, J. M., Arrigo, K. R., Lizotte, M. P., Robinson, D. H., Leventer, A., et al. (2000). Rapid and early export of *Phaeocystis antarctica* blooms in the Ross Sea, Antarctica. *Nature*, *404*(6778), 595–598. https://doi.org/10.1038/35007061

Ducklow, H., Carlson, C., Church, M., Kirchman, D., Smith, D., & Steward, G. (2001). The seasonal development of the bacterioplankton bloom in the Ross Sea, Antarctica, 1994-1997. *Deep-Sea Research II*, *48*(19–20), 4199–4221. https://doi.org/10.1016/S0967-0645(01)00086-8

Dunbar, R. B., Leventer, A. R., & Mucciarone, D. A. (1998). Water column sediment fluxes in the Ross Sea, Antarctica: Atmospheric and sea ice forcing. *Journal of Geophysical Research*, *103*(C13), 30741–30759. https://doi.org/10.1029/1998JC900001

Emerson, S., Stump, C., & Nicholson, D. (2008). Net biological oxygen production in the ocean: Remote in situ measurements of O_2 and N_2 in surface waters. *Global Biogeochemical Cycles*, *22*(3), GB3023. https://doi.org/10.1029/2007GB003095

Gardner, W. D., Richardson, M. J., & Smith, W. O., Jr. (2000). Seasonal patterns of water column particulate organic carbon and fluxes in the Ross Sea, Antarctica. *Deep-Sea Research II*, *47*(15–16), 3424–3449. https://doi.org/10.1016/S0967-0645(00)00074-6

Gruber, N., Landschützer, P., & Lovenduski, N. S. (2019). The variable Southern Ocean carbon sink. *Annual Review of Marine Science*, *11*(1), 159–186. https://doi.org/10.1146/annurev-marine-121916-063407

Guidi, L., Stemmann, I., Jackson, G. A., Ibanez, F., Claustre, H., Legendre, L., et al. (2009). Effects of phytoplankton community on production, size, and export of large aggregates: A world-ocean analysis. *Limnology and Oceanography*, *54*(6), 1951–1963. https://doi.org/10.4319/lo.2009.54.6.1951

Hales, B., & Takahashi, T. (2004). High-resolution biogeochemical investigation of the Ross Sea, Antarctica, during the AESOPS (U.S. JGOFS) program. *Global Biogeochemical Cycles*, *18*(3), GB3006. https://doi.org/10.1029/2003GB002165

Hansell, D. A., & Carlson, C. A. (1998). Net community production of dissolved organic carbon. *Global Biogeochemical Cycles*, *12*(3), 443–453. https://doi.org/10.1029/98gb01928

Henson, S., Le Moigne, F., & Geiring, S. (2019). Drivers of carbon export efficiency in the global ocean. *Global Biogeochemical Cycles*, *33*(7), 891–903. https://doi.org/10.1029/2018GB006158

Henson, S. A., Cael, B. B., Allen, S. R., & Dutkiewicz, S. (2021). Future phytoplankton diversity in a changing climate. *Nature Communications*, *12*(1), 5372. https://doi.org/10.1038/s41467-021-25699-w

Jones, R. M. (2015). *The influence of short-term events on the hydrographic and biological structure of the southwestern Ross Sea*. M.S. Thesis, William & Mary.

Jones, R. M., & Smith, W. O., Jr. (2017). The influence of short-term events on the hydrographic and biological structure of the southwestern Ross Sea. *Journal of Marine Systems*, *166*, 184–195. https://doi.org/10.1016/j.jmarsys.2016.09.006

Juranek, L. W., White, A. E., Dugenne, M., Henderikx Freitas, F., Dutkiewicz, S., Ribalet, F., et al. (2020). The importance of the phytoplankton "middle class" to ocean net community production. *Global Biogeochemical Cycles*, *34*(12), e2020GB006702. https://doi.org/10.1029/2020GB006702

Kalnay, E., Kanamitsu, M., Kistler, R., Collins, W., Deaven, D., Gandin, L., et al. (1996). The NCEP/NCAR 40-year reanalysis project. *Bulletin of the American Meteorology Society*, *77*(3), 437–470. https://doi.org/10.1175/1520-0477(1996)077<0437:tnyrp>2.0.co;2

Kaufman, D. E., Friedrichs, M. A. M., Hennings, J. C. P., & Smith, W. O., Jr. (2018). Assimilating bio-optical glider data: Time and space variability during a phytoplankton bloom in the southern Ross Sea. *Biogeosciences*, *15*, 73–90. https://doi.org/10.5194/bg-15-73-2018

Kaufman, D. E., Friedrichs, M. A. M., Smith, W. O., Jr., Hofmann, E. E., Dinniman, M. S., & Hennings, J. C. P. (2017). Climate change impacts on Ross Sea biogeochemistry: Results from 1D modeling experiments. *Journal of Geophysical Research: Oceans*, *122*(3), 2339–2359. https://doi.org/10.1002/2016JC012514

Kaufman, D. E., Friedrichs, M. A. M., Smith, W. O., Jr., Queste, B. Y., & Heywood, K. J. (2014). Biogeochemical variability in the southern Ross Sea as observed by a glider deployment. *Deep-Sea Research I*, *92*, 93–106. https://doi.org/10.1016/j.dsr.2014.06.011

Lacour, L., Briggs, N., Claustre, H., Ardyna, M., & Dall'Olmo, G. (2019). The intraseasonal dynamics of the mixed layer pump in the subpolar North Atlantic Ocean: A Biogeochemical-Argo float approach. *Global Biogeochemical Cycles*, *33*(3), 266–281. https://doi.org/10.1029/2018GB005997

Langone, L., Frignani, M., Cochran, J. K., & Ravaioli, M. (1997). Scavenging processes and export fluxes close to a retreating seasonal ice margin (Ross Sea, Antarctica). *Water, Air, and Soil Pollution*, *99*, 177–201. https://doi.org/10.1007/978-94-0115552-6_72

Laws, E. A. (1991). Photosynthetic quotients, new production and net community production in the open ocean. *Deep-Sea Research*, *38*(1), 143–167. https://doi.org/10.1016/0198-0149(91)90059-o

Laws, E. A., & Maiti, K. (2019). The relationship between primary production and export production in the ocean: Effects of time lags and temporal variability. *Deep-Sea Research I*, *148*, 100–107. https://doi.org/10.1016/j.dsr.2019.05.006

Le Quere, C., Rodenbeck, C., Buitenhuis, E. T., Conway, T. J., Langenfelds, R., Gomez, A., et al. (2007). Saturation of the Southern Ocean CO_2 sink due to recent climate change. *Science*, *316*(5832), 1735–1738. https://doi.org/10.1126/science.1136188

Liang, J., Deutsch, C., McWilliams, J. C., Baschek, B., Sullivan, P. P., & Chiba, D. (2013). Parameterizing bubble-mediated air-sea gas exchange and its effect on ocean ventilation. *Global Biogeochemical Cycles*, *27*(3), 894–905. https://doi.org/10.1002/gbc.20080

Long, M. C., Dunbar, R. B., Tortell, P. D., Smith, W. O., Jr., Mucciarone, D. A., & DiTullio, G. R. (2011). Vertical structure, seasonal drawdown, and net community production in the Ross Sea, Antarctica. *Journal of Geophysical Research*, *116*(C10), C10029. https://doi.org/10.1029/2009JC005954

Martin, J. H., Knauer, G. A., Karl, D. M., & Broenkow, W. W. (1987). VERTEX: Carbon cycling in the northeast Pacific. *Deep-Sea Research I*, *34*(2), 267–285. https://doi.org/10.1016/0198-0149(87)90086-0

Mathot, S., Smith, W. O., Jr., Carlson, C. A., Garrison, D. L., Gowing, M. M., & Vickers, C. L. (2000). Estimate of *Phaeocystis* sp. carbon biomass: Methodological problems related to the mucilaginous nature of the colonial matrix. *Journal of Phycology*, *36*(6), 1049–1056. https://doi.org/10.1046/j.1529-8817.2000.99078.x

Morel, A. (1974). Optical properties of pure water and pure seawater. In N. G. Jerlov & E. Steemann Nielsen (Eds.), *Optical aspects of oceanography* (pp. 1–24). Academic.

Naegler, T., Ciais, P., Rodgers, K., & Levin, I. (2006). Excess radiocarbon constraints on air-sea gas exchange and the uptake of CO_2 by the oceans. *Geophysical Research Letters*, *33*(11), L11802. https://doi.org/10.1029/2005GL025408

Nelson, D. M., DeMaster, D. J., Dunbar, R. B., & Smith, W. O., Jr. (1996). Cycling of organic carbon and biogenic silica in the Southern Ocean: Estimates of water-column and sedimentary fluxes on the Ross Sea continental shelf. *Journal of Geophysical Research*, *101*(C8), 18519–18532. https://doi.org/10.1029/96JC01573

Queste, B. (2015). UEA Seaglider Toolbox. Bitbucket. Retrieved from https://bitbucket.org/bastienqueste/uea-seaglider-toolbox/

Queste, B. Y., Heywood, K. J., Smith, W. O., Jr., Kaufman, D. E., Jickells, T. D., & Dinniman, M. S. (2015). Dissolved oxygen dynamics during a phytoplankton bloom in the Ross Sea polynya. *Antarctic Science*, *27*(4), 362–372. https://doi.org/10.1017/S0954102014000881

Reigstad, M., & Wassmann, P. (2007). Does *Phaeocystis* spp. contribute significantly to vertical export of organic carbon? *Biogeochemistry*, *83*(1–3), 217–234. https://doi.org/10.1007/s10533-007-9093-3

Ryan-Keogh, T., & Smith, W. O., Jr. (2021). Temporal patterns of iron limitation in the Ross Sea as determined from chlorophyll fluorescence. *Journal of Marine Systems*, *215*, 103500. https://doi.org/10.1016/j.jmarsys.2020.103500

Salle, J. B., Speer, K., Rintoul, S., & Wijffels, S. (2010). Southern Ocean thermocline ventilation. *Journal of Physical Oceanography*, *40*(3), 509–529. https://doi.org/10.1175/2009JPO4291.1

Schine, C. M. S., van Dijken, G., & Arrigo, K. R. (2015). Spatial analysis of trends in primary production and relationship with large-scale climate variability in the Ross Sea, Antarctica (1997–2013). *Journal of Geophysical Research: Oceans*, *121*(1), 368–386. https://doi.org/10.1002/2015JC011014

Smith, W. O., Jr., Ainley, D. G., Arrigo, K. R., & Dinniman, M. S. (2014). The oceanography and ecology of the Ross Sea. *Annual Review of Marine Science*, *6*(1), 469–487. https://doi.org/10.1146/annurev-marine-010213-135114

Smith, W. O., Jr., Asper, V. L., Tozzi, S., Liu, X., & Stammerjohn, S. E. (2011). Surface layer variability in the Ross Sea, Antarctica as assessed by in situ fluorescence measurements. *Progress in Oceanography*, *88*(1–4), 28–45. https://doi.org/10.1016/j.pocean.2010.08.002

Smith, W. O., Jr., & Dunbar, R. B. (1998). The relationship between new production and vertical flux on the Ross Sea continental shelf. *Journal of Marine Systems*, *17*(1–4), 445–457. https://doi.org/10.1016/S0924-7963(98)00057-8

Smith, W. O., Jr., Goetz, K. T., Kaufman, D. E., Queste, B. Y., Asper, V., Costa, D. P., et al. (2014). Multi-platform, multi-disciplinary investigations of the Ross Sea, Antarctica. *Oceanography*, *27*, 180–185. Retrieved from http://www.jstor.org/stable/24862169

Smith, W. O., Jr., & Gordon, L. I. (1997). Hyperproductivity of the Ross Sea (Antarctica) polynya during austral spring. *Geophysical Research Letters*, *24*(3), 233–236. https://doi.org/10.1029/96GL03926

Smith, W. O., Jr., & Kaufman, D. E. (2018). Climatological temporal and spatial distributions of nutrients and particulate matter in the Ross Sea. *Progress in Oceanography*, *168*, 182–195. https://doi.org/10.1016/j.pocean.2018.10.003

Smith, W. O., Jr., Marra, J., Hiscock, M. R., & Barber, R. T. (2000). The seasonal cycle of phytoplankton biomass and primary productivity in the Ross Sea, Antarctica. *Deep-Sea Research II*, *47*(15–16), 3119–3140. https://doi.org/10.1016/S0967-0645(00)00061-8

Smith, W. O., Jr., Shields, A. R., Dreyer, J., Peloquin, J. A., & Asper, V. (2011). Interannual variability in vertical export in the Ross Sea: Magnitude, composition, and environmental correlates. *Deep-Sea Research I*, *58*(2), 147–159. https://doi.org/10.1016/j.dsr.2010.11.007

Smith, W. O., Jr., Shields, A. R., Peloquin, J. A., Catalano, G., Tozzi, S., Dinniman, M. S., & Asper, V. A. (2006). Interannual variations in nutrients, net community production, and biogeochemical cycles in the Ross Sea. *Deep-Sea Research II*, *53*(8–10), 815–833. https://doi.org/10.1016/j.dsr2.2006.02.014

Smith, W. O., Jr., Tozzi, S., Long, M. C., Sedwick, P. N., Peloquin, J. A., Dunbar, R. B., et al. (2013). Spatial and temporal variations in variable fluorescence in the Ross Sea (Antarctica): Oceanographic correlates and bloom dynamics. *Deep-Sea Research I*, *79*, 141–155. https://doi.org/10.1016/j.dsr.2013.05.002

Steinberg, D. K., Van Mooy, B. A. S., Buesseler, K. O., Boyd, P. W., Kobari, T., & Karl, D. M. (2008). Bacterial vs. zooplankton control of sinking particle flux in the ocean's twilight zone. *Limnology and Oceanography*, *53*(4), 1327–1338. https://doi.org/10.4319/lo.2008.53.4.1327

Sweeney, C., Hansell, D. A., Carlson, C. A., Codispoti, L. A., Gordon, L. I., Marra, J., et al. (2000). Biogeochemical regimes, net community production and carbon export in the Ross Sea, Antarctica. *Deep-Sea Research II*, *47*(15–16), 3369–3394. https://doi.org/10.1016/S0967-0645(00)00072-2

Turner, J. T. (2002). Zooplankton fecal pellets, marine snow and sinking phytoplankton blooms. *Aquatic Microbial Ecology*, *27*, 57–102. https://doi.org/10.3354/ame027057

Twinning, B. S., Nodder, S. D., King, A. L., Hutchins, D. A., LeCleir, G. R., DeBruyn, J. M., et al. (2014). Differential remineralization of major and trace elements in sinking diatoms. *Limnology and Oceanography*, *59*(3), 689–704. https://doi.org/10.4319/lo.2014.59.3.0689

Wanninkhof, R. (1992). Relationship between wind speed and gas exchange over the ocean. *Journal of Geophysical Research*, *97*(C5), 7373–7382. https://doi.org/10.1029/92jc00188

Yang, B., Emerson, S. R., & Bushinsky, S. M. (2017). Annual net community production in the subtropical Pacific Ocean from in situ oxygen measurements on profiling floats. *Global Biogeochemical Cycles*, *31*(4), 728–744. https://doi.org/10.1002/2016GB005545

Yasuda, S., Tkagi, T., Naraoka, H., Kitajima, F., & Takahashi, K. (2016). Carbon isotope ratios of organic matter in Bering Sea settling particles: Extremely high remineralization of organic carbon derived from diatoms. *Geochemistry Journal*, *50*(3), 241–248. https://doi.org/10.2343/geochemj.2.0411